JSCAI
The official journal of the Society for Cardiovascular Angiography & Interventions

Original Research

Tibial Artery Stent Deformations From Ankle Plantarflexion and Dorsiflexion, Knee Flexion, and Simulated Calf Muscle Contraction

Christopher P. Cheng, PhD [a,*], Johan Bondesson, PhD [a], Anna Johnson [a], Stanley K. Zimmerman, MD [b]

[a] Division of Vascular Surgery, Department of Surgery, Stanford University, Stanford, California; [b] Oklahoma Heart Institute, Department of Interventional Cardiology, Tulsa, Oklahoma

ABSTRACT

Background: Tibial artery stent deformations have not been previously published and are critical for the evaluation and development of below-the-knee treatments.

Methods: Balloon-expandable stents were implanted into the anterior tibial, posterior tibial, and peroneal arteries of cadaver legs, including ostium-crossing locations. Computed tomography and geometric modeling were used to quantify cross-sectional, axial, and bending stent deformations from ankle plantarflexion/dorsiflexion, knee flexion, and simulated calf muscle contraction for walking/running.

Results: Single and overlapping stents (N = 53) were deployed into 23 tibial arteries and across 6 ostia. Diametric crush was experienced in the posterior tibial with knee flexion (–5.3% ± 3.2%, $P < .0001$) and peroneal with ankle dorsiflexion (–2.4% ± 2.0%, $P = .0016$), and posterior tibial stents experienced greater diametric crush from knee flexion (–5.3% ± 3.2%) and calf compression (–3.4% ± 5.9%) compared to ankle motion (–0.2% ± 4.3%; $P = .0009$ and $P = .0061$, respectively). Ostium-crossing stents experienced order of magnitude higher axial shortening with knee flexion and ankle plantarflexion compared to those in single arteries. No stent bending was observed from any leg motion.

Conclusions: Diametric crush in posterior tibial and peroneal stents was potentially due to their location in the deep posterior compartment and adjacent to the soleus/gastrocnemius muscles that bulge with joint motion. Crush in the posterior tibial is greater for knee flexion and calf compression compared to ankle motion from a higher bone-to-muscle ratio near the ankle protecting against crush. Ostium-crossing stents experience larger shortening than those in individual arteries potentially because of a more oblique orientation. No significant stent bending was observed possibly because the midcalf is distant from knee and ankle joints and protected by the rigid tibia and fibula. These stent deformations can guide device development, interventional site selection, and indications for use.

Introduction

Lower extremity occlusive artery disease has been estimated to affect more than 202 million people globally and is a growing problem due to aging populations and increasing incidence of risk factors.[1,2] Due to smaller vessel caliber and severity of disease, vascular disease below the knee (BTK) is more difficult to access and treat compared to above the knee with surgical and/or percutaneous treatments.[3] Furthermore, BTK disease is commonly associated with chronic limb-threatening ischemia, which is concomitant with high morbidity (eg, rest pain, nonhealing wounds, limb loss), and if not properly treated, very expensive long-term multidisciplinary care (eg, podiatry, wound care, amputation, loss of mobility).[4] As such, there has been an increase in the adoption of interventional treatments for BTK vascular treatments including drug-coated balloons, atherectomy, intravascular lithotripsy, stenting, and deep venous arterialization.[3,5] Supported by a growing body of evidence, stenting, which has traditionally been reserved as a bailout strategy, is now being suggested as a primary option for BTK vascular treatments.[6]

In the growing number of cases where stents are implanted into the vasculature, mechanical interactions between the stents and anatomy are of paramount concern regarding device and patency durability, particularly in the face of inadequate current treatments and multiple stent technologies under development.[3,7–10] Although cardiac pulsatility causes pulsatile vascular motion, largely in the cross-sectional dimension, respiration and musculoskeletal motion can cause significant cross-sectional, axial, and bending deformations in the aortic arch

Abbreviations: 2D, two-dimensional; 3D, three-dimensional; ATA, anterior tibial artery; BTK, below the knee; CT, computed tomography; PA, peroneal artery; PTA, posterior tibial artery.

Keywords: device durability; joint flexion biomechanics; peripheral artery disease; stent deformations; tibial artery stenting.

* Corresponding author: cpc@stanford.edu (C.P. Cheng).

https://doi.org/10.1016/j.jscai.2024.102522
Received 3 September 2024; Received in revised form 17 December 2024; Accepted 20 December 2024; Available online 23 January 2025
2772-9303/© 2024 The Author(s). Published by Elsevier Inc. on behalf of the Society for Cardiovascular Angiography & Interventions Foundation. This is an open access article under the CC BY-NC-ND license (http://creativecommons.org/licenses/by-nc-nd/4.0/).

branches,[11] carotid arteries,[12] renovisceral arteries,[13] femoropopliteal arteries,[14–16] and iliofemoral veins.[17] The muscle pressures in the lower leg can get extremely high (~300 mm Hg) because the entire body weight during upright locomotion is supported by the relatively small cross-section of musculoskeletal structures in the calf[1,18,19]; however, quantitative tibial artery deformations due to musculoskeletal motion have not yet been reported in the literature.

The distal tibial arteries near the ankle (where the anterior tibial transitions to the dorsalis pedis, and posterior tibial approaches the heel) have been qualitatively shown to experience kinking during ankle flexion and extension via 2D angiograms.[20] Relatedly, stents implanted into the distal anterior tibial and posterior tibial arteries are suspected to be at increased risk of compression and fracture due to direct contact with the rigid tibia while being crossed by the musculotendinous (eg, extensor hallucis longus, extensor digitalis longus) and ligament structures.[21] Although the proximal tibial arteries may be distant enough from the ankle joint to avoid deformation due to ankle motion, they may be influenced by knee flexion or the strong, compartmentalized muscles of the calf, especially during the weight-bearing muscle contraction of plantarflexion. To address this, we propose a cadaver study where balloon-expandable cobalt-chromium coronary stents are implanted into the proximal two-thirds of the anterior tibial, posterior tibial, and peroneal arteries, and then their deformations resulting from aggressive ankle and knee joint motions, as well as simulated calf muscle contraction, are quantified.

Methods

Cadaver study and medical imaging

The cadaver study was performed at the Medical Education & Research Institute (Memphis, TN), utilizing both the right and left legs of 4 fresh cadavers, with each cadaver leg harvested from femoral head to toe. IRB approval was not required as no patients were involved. Cadavers were selected to include 2 male cadavers and 2 female cadavers, ranging in height from <5′4″ to >6′0″, and be free of lower extremity occlusive vascular disease. A 9F introducer sheath was placed in the femoral artery and the cannulated femoral artery was tied off with a suture to enable pressurization. A 2-way stopcock was utilized with one port connected to a pressurized 3 L hanging saline intravenous bag (pressure adjustable with line roller clamp), and the second port connected to a pressure gauge.[17] In preparation for implanting the stents into the anterior tibial, posterior tibial, and peroneal arteries, hydrophilic guide wires were placed into the vessels through the sheath.

All medical imaging was performed using a C-arm with 3D rotational computed tomography (CT) capabilities (ARTIS pheno C-arm Angiography System, Siemens Healthcare). While the vessels were pressurized to arterial pressure, 50/50 contrast/saline was injected through the introducer sheath, and a 2D angiogram was obtained for vessel sizing and stent selection. All implants were balloon-expandable cobalt-chromium drug-eluting stents indicated for the coronary arteries (Resolute Onyx DES, Medtronic) and were implanted into the proximal two-thirds of the tibial arteries. The stent configurations were chosen to be common clinical use conditions, with a preference for longer stented segments and overlapped stents because they correlate with greater deformation and incidence of stent fracture.[7-9]

Stenting was performed in a clinically relevant manner by an experienced peripheral vascular interventionalist in all 3 tibial arteries as well as a subset crossing the various tibial artery ostia. Stents not intended to cross the ostia were placed at least 10 mm away from the ostia and overlapping stents were overlapped at least 5 mm with the distal stent deployed first. Stent diameter and inflation pressure were chosen to target an oversizing ratio of 1.1 (10% overstretch) at the midpoint of the segment to be treated, with final discretion and decision-making performed by the interventionalist.

After stenting, 3D rotational CT images were taken with simultaneous arterial pressurization. Pressurization of 60 mm Hg was selected as a low-end arterial pressure because lower arterial pressure should promote greater stent deformation and the resulting deformations could be considered conservative. While maintaining pressure, each leg was imaged in the joint positions (using an adjustable radiolucent peg board) and external calf pressurizations (using a pressure cuff) as shown in Figure 1, following the same order of serial manipulations for all 8 legs. The manipulations were done in a serial manner, rather than returning to a neutral position in between each manipulation, to minimize the number of manipulations and time because more saline pressurization would have increased edema and difficulty of joint motion, as well as make the motion less physiologically relevant. To encompass the full range of ankle motion, neutral, maximum dorsiflexion, and maximum plantarflexion positions were imaged both with the knee straight (positions 1-3) and flexed 90° (positions 4-6). In addition, a blood pressure cuff was placed on the calf spanning the stented region and was inflated to exert pressures of 100, 200, and 300 mm Hg (positions 7-9) to simulate maximum intramuscular contraction pressures in the superficial posterior, deep posterior, anterior, and lateral compartments for standing,[22] walking,[23] and running,[18,23] respectively.

Geometric modeling and deformation quantification

Using custom vascular modeling software (SimVascular, github.com/SimVascular) on the postimplant 3D CT images, approximate centerline paths of the stents were selected manually (Figure 2, left).[24] These approximate paths were then used as the basis for defining orthogonal planes on which to perform 2D segmentations of the stent cross-sections (Figure 2, middle). Segmentations were spaced approximately 10 mm apart along the length while making sure to capture the ends of each stent. Next, the centroids of the 2D segmentations were splined and optimally Fourier-smoothed to compute true stent centerline paths.[25] The contours of each stent model were lofted to form a 3D stereolithography surface model (Figure 2, right).

Geometric quantification of stents included cross-sectional minor diameter, centerline axial length, and centerline curvature (Figure 2, right).[17,25] Minor diameter was calculated as the minimum diameter of the cross-section passing through the centroid of the contour. These contours were spaced at ≤10 mm intervals and minor diameter was length-averaged for the stented segment. Axial length was defined as the centerline arc length between 2 fiducial markers, eg, 2 ends of a stented segment. Curvature was defined as the inverse of the radius of curvature of the centerline, where the radius was defined by a circumscribed circle fit onto 3 equispaced centerline path points within a window size of 10 mm. Curvature was calculated along the centerline at 1 mm increments.

These metrics were calculated and compared between different leg positions and cuff pressurizations to quantify deformations due to leg motions relevant for locomotion (Table 1). These motions include ankle plantarflexion and dorsiflexion with a straight knee, ankle plantarflexion and dorsiflexion with a flexed knee, knee flexion with a neutral ankle, maximum change in calf muscle length, and various amounts of calf muscle contraction. To calculate maximum localized changes in stent curvature between leg positions, the curvatures at pairwise material points along the stent were compared by matching material points with a dynamic time-warping technique.[26,27]

Statistics

Cohort stent deformation for relevant leg motions was reported as mean ± SD for length-averaged minor diameter, axial arc length, and maximum localized change in curvature. Two-tailed unpaired *t* tests were performed between leg positions to identify significant stent deformations, with a statistical significance threshold set at $P <$

Figure 1.
Images of cadaver leg positions. Leg positions were constrained with a radiolucent peg board with various combinations of knee and ankle joint flexion (positions 1-6), and external calf compressions (positions 7-9) to simulate common modes of locomotion. Each leg was manipulated serially in the same order from positions 1 through 6.

.05 and then adjusted for multiple comparisons by Bonferroni-Holm correction.[28] Two-tailed unpaired *t* tests were also performed between the stent deformations of different artery locations, and between different leg motions, to identify whether certain tibial arteries or motions exhibited significantly greater stent deformations compared to others.

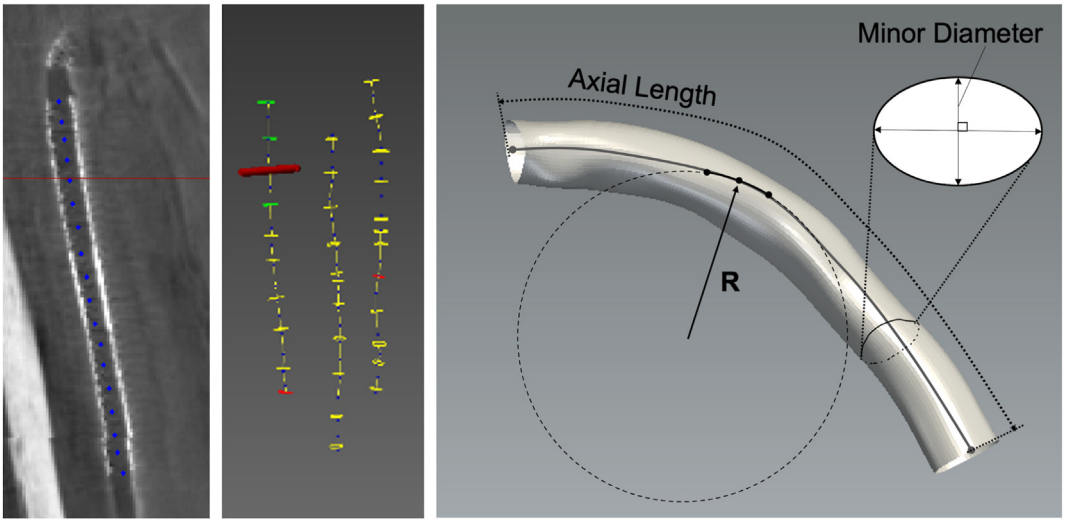

Figure 2.
Overview of modeling and quantification steps. Centerline points were manually selected along the length of 2 overlapped stents (left). Centerline points were used to create centerline paths of overlapped stents in the anterior tibial, posterior tibial, and peroneal arteries, along which orthogonal cross-sections were constructed (middle). These cross-sectional contours were lofted together to form 3D geometric models of the stents, from which cross-sectional minor diameter, axial arc length, and centerline curvature were calculated (right).

Results

Cadaver details and implant matrix

In 8 cadaver legs, 53 balloon-expandable stents were deployed into 8 anterior tibial, 7 posterior tibial, and 8 peroneal arteries, as well as across 6 artery ostia (Table 2). For visualization purposes, the stent geometric models of all leg positions, for example, right and left legs, were coregistered by translation and rotation operations to depict their relative positions and geometries to each other (Central Illustration).

Tibial stent deformations

During CT imaging of various leg positions and calf pressurizations, no stent deformation or migration was visually obvious with knee and ankle joint manipulation or calf compression. Cohort-averaged minor diameter, axial arc length, and maximum localized bending stent deformations for the anterior tibial, posterior tibial, peroneal, and crossing ostia locations for leg motions relevant to locomotion are shown in Table 3. There was significant diametric stent compression for the anterior tibial artery with 200 mm Hg calf compression (–4.8% ± 5.2%, $P = .0091$), for the posterior tibial artery with knee flexion (–5.3% ± 3.2%, $P < .0001$), and for the peroneal artery with ankle dorsiflexion (–2.4% ± 2.0%, $P = .0016$). There was significant stent lengthening in the posterior tibial artery (200 mm Hg = 1.4% ± 1.4%, $P = .0052$; 300 mm Hg = 1.7% ± 1.6%, $P = .0046$) and in ostium-crossing locations (200 mm Hg = 3.7% ± 2.5%, $P = .0051$) with calf compression. Finally, there was significant stent shortening in the peroneal artery with knee flexion (–1.6% ± 1.7%, $P = .0072$), and in ostium-crossing stents with knee flexion (–4.1% ± 3.0%, $P = .0082$) and knee flexion combined with ankle plantarflexion (–3.0% ± 1.9%, $P = .0041$). No significant stent bending was observed.

When comparing deformations of stents implanted into the anterior tibial, posterior tibial, peroneal, and ostium-crossing locations, there were no significant differences in motion-induced diametric crush or maximum bending deformations (Table 3). However, ostium-crossing stents experienced significantly greater axial shortening compared to those in the posterior tibial with knee flexion (–4.1% ± 3.0% vs –0.2% ± 1.3%, $P = .0050$), and greater axial shortening compared to those in all 3 tibial arteries with knee flexion combined with ankle plantarflexion (–3.0% ± 1.9% vs anterior = –0.3% ± 1.3%, $P = .0082$; posterior = –0.5% ± 1.6%, $P = .0248$; peroneal = 0.2% ± 2.2%, $P = .0181$).

When comparing deformations of stents between different leg motions, there were no significant differences in diametric, axial, or bending deformations for the peroneal or ostium-crossing locations. Also, there were no significant differences in stent maximum bending for any of the anatomic locations. There was significantly greater diametric crush with calf compression compared to ankle joint motion for anterior tibial stents (calf compression = –4.8% ± 5.9% vs ankle motion = –0.9% ± 3.7%, $P = .0005$) and posterior tibial stents (calf compression = –3.4% ± 5.9% vs ankle motion = –0.2% ± 4.3%, $P = .0061$). The posterior tibial stents also experienced significantly greater diametric crush due to knee flexion compared to ankle motion (knee flexion = –5.3% ± 3.2% vs ankle motion = –0.2% ± 4.3%, $P = .0009$), and lengthened significantly more with calf compression compared to ankle motion (calf compression = 1.3% ± 1.5% vs ankle motion = –0.4% ± 1.4%, $P < .0001$).

Table 1. Leg position changes relevant for locomotion.

Position change	Motion description
0neut →0plant	Plantarflexion of ankle with straight knee
0neut → 0dorsi	Dorsiflexion of the ankle with a straight knee
0plant → 0dorsi	Plantarflex to dorsiflex ankle with a straight knee
90neut → 90plant	Plantarflexion of ankle with flexed knee
90neut → 90dorsi	Dorsiflexion of ankle with flexed knee
90plant → 90dorsi	Plantarflex to dorsiflex ankle with flexed knee
0neut → 90neut	Flexion of the knee with a neutral ankle
0dorsi → 90plant	Longest calf muscle position to shortest calf muscle position
0neut → 100 mm Hg	100 mm Hg isometric calf contraction with a straight knee and neutral ankle
0neut → 200 mm Hg	200 mm Hg isometric calf contraction with a straight knee and neutral ankle
0neut → 300 mm Hg	300 mm Hg isometric calf contraction with a straight knee and neutral ankle

Knee bend angle is denoted by 0 or 90 meaning 0° or 90°, respectively. Ankle bend is denoted by neut, plant, or dorsi, referring to neutral, dorsiflex, or plantarflex ankle, respectively. Calf pressurization is denoted by 100 mm Hg, 200 mm Hg, and 300 mm Hg, each referring to the leg at 0° knee with a neutral ankle, and pressure cuff compression around the calf.

Table 2. Cadaver details and stent implant matrix.

#	Demographics	Leg	Anterior tibial	Posterior tibial	Peroneal	Ostium crossing
1	80 y, male, 5′9″, 160 lb	Right	4.0 × 38 & 4.0 × 38	4.0 × 38 & 4.0 × 38	3.5 × 38 & 4.0 × 38	4.0 × 38 peroneal
		Left	4.0 × 38 & 4.0 × 38	4.0 × 38 & 4.0 × 38	4.0 × 38 & 4.0 × 38	NA
2	64 y, female, 5′3″, 239 lb	Right	3.5 × 38 & 3.5 × 38	2.5 × 38 & 2.5 × 38	3.0 × 38 & 3.5 × 38	3.5 × 38 anterior
		Left	2.5 × 38 & 3.0 × 38	2.5 × 38 & 3.0 × 38	2.5 × 38 & 3.0 × 38	3.5 × 38 anterior
3	77 y, male, 6′2″, 190 lb	Right	2.5 × 38/2.5 × 38	3.5 × 38/4.0 × 38	3.0 × 38/3.5 × 38	4.0 × 38 TP trunk
		Left	2.5 × 38/2.5 × 38	2.5 × 38/3.0 × 38	2.5 × 38/3.0 × 38	4.0 × 38 TP trunk
4	93 y, female, 5′2″, 168 lb	Right	3.0 × 38 & 3.0 × 38	2.25 × 38 & 2.25 × 38 NA	2.5 × 38 & 2.5 × 38	2.5 × 38 posterior
		Left	2.5 × 38 & 3.0 × 38		2.25 × 38 & 2.25 × 38	NA

Stent dimensions in diameter × length (mm). When 2 stents are listed, the first is distal and the second is proximal.
&, 2 overlapped stents; /, 2 single stents; TP trunk, tibioperoneal trunk.

Discussion

Precise quantification of stent geometries with leg manipulations revealed statistically significant stent deformations; however, even with physiologically aggressive knee and ankle joint manipulation, and up to 300 mm Hg of calf compression, it was difficult to detect stent deformation by visual inspection, supporting the need for precise geometric modeling and deformation quantification.

Stent diametric deformations

The average minor diameter compression due to all knee and ankle joint movements was only statistically significant in the posterior tibial for 90° knee flexion and in the peroneal for maximum ankle dorsiflexion. This may be because, at the midcalf level, the posterior tibial and peroneal arteries are in the deep posterior compartment of the calf residing adjacent to the soleus muscle, which is the largest muscle at the midcalf level and may deform the most by passive joint motion. The crush of the posterior tibial artery from knee flexion may also be due to concomitant contraction of the gastrocnemius, which is in the superficial posterior compartment.

Aggressive calf compression (200 mm Hg) causes significant diametric compression only in anterior tibial stents, perhaps because the anterior tibial artery is the most superficial of the tibial arteries at the calf, and most susceptible to external compression. This is corroborated by the fact that diametric crush was significantly greater for calf compression compared to ankle joint motion for anterior tibial stents. In the posterior tibial artery, both knee flexion and calf compression caused significantly greater diametric stent compression compared to ankle joint motion. Again, posterior tibial compression from knee flexion could partially be a consequence of gastrocnemius bulging. Knee flexion and calf compression may have more dominant diametric effects than ankle joint motion on the posterior tibial artery simply because of the larger proportion of muscle-to-bone cross-section ratio

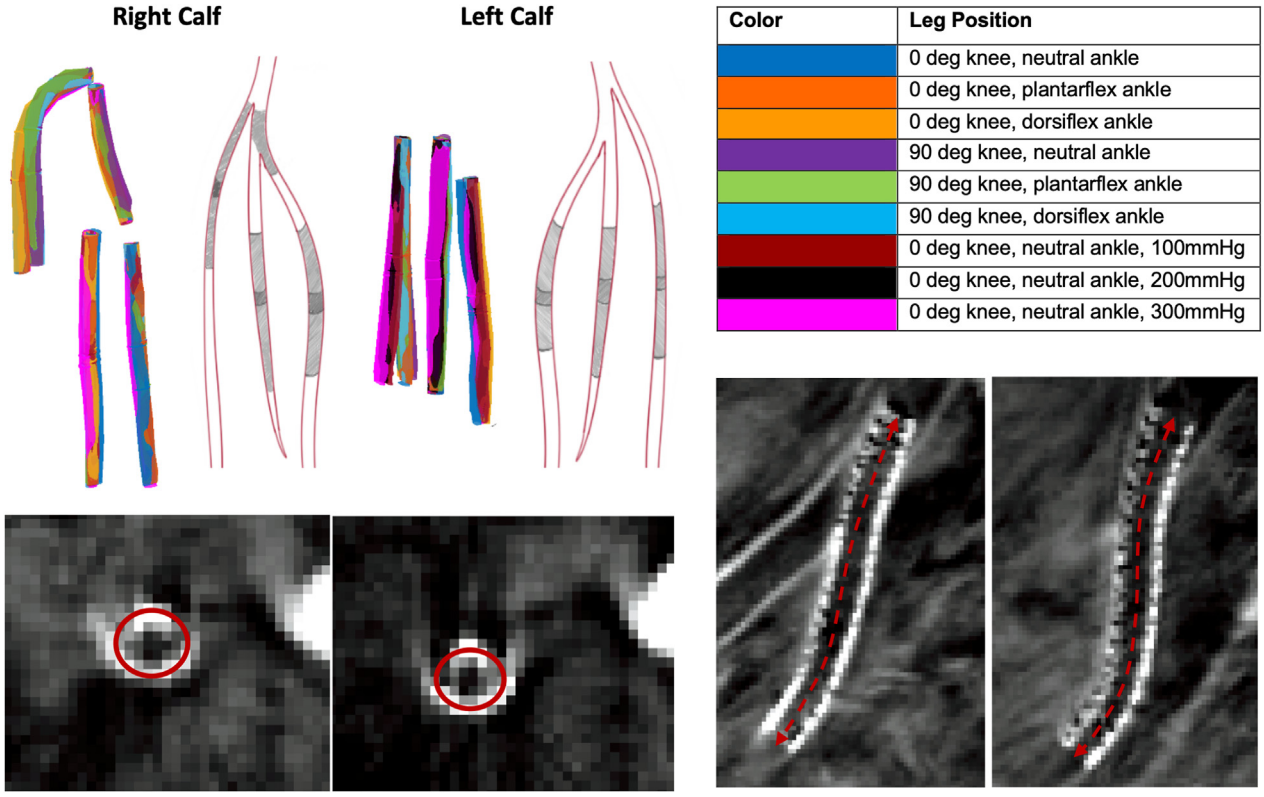

Central Illustration.
Coregistered geometric stent models and matching implant schematics for right and left legs of cadaver #1 (top left), color-coded by joint position and external calf pressurization (top right). This example shows 2 overlapped stents in each of the anterior tibial, posterior tibial, and peroneal arteries of both the right and left legs, and a single stent crossing the peroneal ostium in the right leg. The bottom graphics show paired computed tomography images depicting diametric crush from neutral position to 300 mm Hg pressurization (bottom left, –10.6% change in minor diameter) and arc length lengthening from neutral position to straight knee with ankle dorsiflexion (bottom right, +4.8% change in centerline length).

Table 3. Minor diameter, arc length, and maximum localized bending deformations of stents in the anterior tibial, posterior tibial, peroneal, and ostium-crossing locations for relevant leg motions.

Position change	Minor diameter change, %				Arc length change, %				Max localized bending, cm^{-1}			
	ATA	PTA	PA	Ostia	ATA	PTA	PA	Ostia	ATA	PTA	PA	Ostia
0neut → 0plant	1.1 ± 3.3	–0.8 ± 3.9	–0.7 ± 6.2	–0.8 ± 9.2	–0.5 ± 1.6	–0.7 ± 1.2	–1.2 ± 1.5	–1.0 ± 3.7	0.02 ± 0.10	0.02 ± 0.10	0.03 ± 0.10	–0.03 ± 0.21
0neut → 0dorsi	–1.7 ± 3.6	–2.5 ± 4.4	–1.3 ± 7.2	–0.9 ± 8.3	–0.6 ± 1.2	–0.4 ± 0.7	–1.5 ±1.6	1.4 ± 2.5	0.04 ± 0.11	0.00 ± 0.10	0.01 ± 0.11	–0.03 ± 0.25
0plant → 0dorsi	–2.8 ± 3.6	–1.7 ± 3.8	–0.5 ± 5.8	0.0 ± 4.2	–0.1 ± 1.6	0.3 ± 1.1	–0.3 ±1.1	2.5 ± 3.0	0.03 ± 0.13	–0.05 ±0.12	0.01 ± 0.12	0.02 ± 0.24
90neut → 90plant	–1.9 ± 4.2	1.6 ± 4.8	–1.3 ±3.0	–3.3 ±6.8	0.3 ± 1.2	–0.7 ± 1.0	0.3 ±1.3	2.8 ± 5.2	–0.06 ± 0.07	0.01 ±0.08	0.00 ± 0.09	–0.06 ± 0.13
90neut → 90dorsi	–0.9 ± 2.6	2.0 ± 4.5	–2.4 ± 2.0[a]	–3.7 ± 3.5	0.4 ± 1.1	–0.9 ± 1.9	0.1 ±1.6	3.4 ± 4.5	–0.01 ± 0.08	0.01 ±0.08	–0.02 ± 0.10	–0.04 ± 0.25
90plant → 90dorsi	0.7 ± 3.9	0.5 ± 2.9	0.6 ± 6.4	0.0 ± 7.8	–0.1 ± 1.0	–0.1 ± 2.2	–0.3 ± 1.0	0.7 ± 1.0	0.00 ± 0.08	0.00 ±0.09	–0.01 ± 0.10	0.07 ± 0.19
0neut → 90neut	–1.0 ± 3.8	–5.3 ± 3.2[a]	0.0 ±7.2	0.4 ± 6.6	–1.1 ± 1.8	–0.2 ± 1.3[b]	–1.6 ± 1.7[a]	–4.1 ± 3.0[a,b]	0.07 ± 0.13	0.02 ±0.10	0.00 ± 0.11	0.14 ± 0.21
0dorsi → 90plant	–1.1 ± 4.8	–1.3 ± 4.0	0.2 ± 6.2	–2.0 ± 3.9	–0.3 ± 1.3[b]	–0.5 ± 1.6[b]	0.2 ± 2.2[b]	–3.0 ± 1.9[a,b]	–0.05 ± 0.13	0.03 ± 0.09	–0.02 ± 0.10	0.07 ± 0.23
0neut → 100 mm Hg	–3.9 ± 6.3	–2.9 ± 4.9	1.4 ± 12.6	–1.4 ± 9.1	–0.1 ± 2.1	1.0 ± 1.4	–0.4 ± 1.4	1.7 ± 1.5	0.00 ± 0.09	0.00 ±0.10	–0.02 ± 0.08	–0.14 ± 0.15
0neut → 200 mm Hg	–4.8 ± 5.2[a]	–2.2 ± 5.2	–1.3 ± 9.4	–5.0 ± 9.1	0.4 ± 1.7	1.4 ± 1.4[a]	0.7 ± 1.5	3.7 ± 2.5[a]	0.05 ± 0.09	0.00 ±0.10	0.06 ± 0.09	–0.07 ± 0.19
0neut → 300 mm Hg	–5.7 ± 6.7	–5.0 ± 7.5	–4.7 ± 5.5	–3.0 ± 5.6	0.2 ± 2.2	1.7 ± 1.6[a]	0.6 ± 2.7	1.4 ± 2.8	0.02 ± 0.09	–0.01 ±0.10	0.02 ± 0.12	–0.12 ± 0.12

Knee bend angle is denoted by 0 or 90 meaning 0 or 90°, respectively. Ankle bend is denoted by neut, plant, or dorsi, referring to neutral, dorsiflexed, or plantarflexed ankle, respectively. Calf pressurization is denoted by 100 mm Hg, 200 mm Hg, and 300 mm Hg, each referring to the leg at 0° knee with a neutral ankle, and pressure cuff compression around the calf.
ATA, anterior tibial artery; Ostia, ostium-crossing locations; PA, peroneal artery; PTA, posterior tibial artery.
[a] Values denote statistically significant deformations. [b] Values denote significant differences in deformations between anatomic locations.

where the stents reside in the proximal two-thirds of the tibial arteries; in other words, the higher bone ratio near the ankle may protect the tibial arteries from ankle motion-driven diametric crush.

Average resting supine, decubitus, sitting, and standing intramuscular pressures in the superficial posterior, deep posterior, anterior, and lateral compartments never surpass 40 mm Hg, and stay below ~ 60 mm Hg even at 95th percentile values for the population.[18,22,23,29] Thus, pressures in the lower leg muscular compartments during static contraction, even while weight-bearing full body weight, do not exceed arterial pressures and should not cause appreciable cross-sectional deformation of the tibial arteries. However, during dynamic locomotion, the muscular compartment pressures could exceed arterial pressure, especially during running when muscle contractions need to support many multiples of full body weight.[18,23] Specifically, the anterior tibial could be compressed in the anterior compartment, and the peroneal and posterior tibial arteries could be compressed in the superficial and deep posterior compartments. Thus, it is logical that only calf compression pressures above 100 mm Hg cause significant stent deformations.

Stent axial arc length deformations

Posterior tibial and peroneal artery stents lengthened significantly with aggressive calf compression (200 mm Hg), whereas peroneal (knee flexion) and ostium-crossing (knee flexion, knee flexion with ankle plantarflexion) stents shortened significantly with joint motion. In addition, calf compression caused significantly greater stent length changes than ankle joint motion, and ostium-crossing stents experienced greater shortening due to joint motion than the stents residing exclusively in the anterior tibial, posterior tibial, or peroneal arteries. Because knee flexion, either with a neutral ankle or combined with ankle plantarflexion, causes a shortening of the calf muscles, it follows that the lengths of tibial artery stents significantly shorten with these perturbations. It is also understandable for aggressive circumferential calf compression to lengthen tibial artery stents because the compression would cause the length of the calf muscles to increase while their collective diameter decreases.

Although the axial stent length changes were significant in the posterior tibial and peroneal arteries, even the largest deformations were small in magnitude. On the other hand, the ostium-crossing stent deformations were an order of magnitude higher compared to the posterior tibial artery with knee flexion, and an order of magnitude higher compared to all 3 tibial arteries with knee flexion combined with ankle plantarflexion. The greater length changes for the ostium-crossing stents may be due to a more oblique orientation compared to the superior-inferior orientation of the stents exclusively in the anterior tibial, posterior tibial, or peroneal arteries. Specifically, the arc lengths of more oblique stents would be more sensitive to calf shape change due to joint motion and calf compression.

Stent maximum bending deformations

In contrast to the significant cross-sectional and arc length stent deformations in the tibial arteries, no significant bending deformations were observed due to ankle plantarflexion or dorsiflexion, knee flexion, or calf compression, even though the induced joint motions and external compressions were extreme. This is likely because the implantation sites are at the midcalf, situated away from both the knee and ankle joints, and the tibial arteries are predominantly superior-inferior in orientation. The arteries in this portion of lower leg are further protected

from bending by the rigid tibia and fibula, which are also oriented in the superior-inferior direction.

This is contrary to the femoropopliteal segment, which experiences dramatic bending near the knee.[14–16,30] Based on detailed cadaveric dissection, tortuosity observed in the popliteal artery was limited to the supraarticular region (P1), whereas the articular (P2) and infraarticular (P3) regions were largely free from tortuosity.[30] This is because the P2 and P3 regions are highly restricted by the femoral condyles, and between the tibia and medial and lateral heads of the gastrocnemius, respectively. This means that bending of the knee is unlikely to cause tibial artery deformation because the upper popliteal artery takes the brunt of the deformation.

Device development and clinical implications

The musculoskeletal motion-induced stent deformations reported in this study could prescribe the boundary conditions for stent mechanical durability testing and would be particularly relevant for balloon-expandable stents intended for the tibial arteries. Note that the greatest stent diameter, arc length, and bending deformations in the tibial arteries were induced by external calf compression (an analog for muscle contraction), ankle dorsiflexion, and knee flexion, respectively. Although simultaneous, multimodal deformations must be considered for device fatigue evaluation, because calf muscle contraction, ankle dorsiflexion, and maximum knee flexion do not occur concurrently during the gait cycle,[31] these peak deformations are not likely to be superimposed together.

Besides device evaluation, the deformations described here could also be used as a guide for informing future device designs. Also, the significantly different deformations between stents implanted exclusively in the anterior tibial, posterior tibial, or peroneal arteries, versus those that cross an ostium and span 2 different tibial vessels, suggest that physicians can influence stent durability based on specific implant site selection. These differential deformations can similarly inform device indications for use regarding anatomic site selection, and influence regulatory approval decisions.

Limitations

This study included certain limitations including using cadavers with healthy vasculature, small cohort size, absence of active muscle contraction in cadaver specimens, and only using coronary stents from a single manufacturer. Diseased arteries with heavy calcium load could potentially decrease deformations from calcium shielding or increase localized deformations directly adjacent to calcium. A larger cohort would lead to greater confidence in the stent deformation results, as well as likely identify more statistically significant deformations, and differences in deformations because there were several P values $<.05$ that did not qualify as significant after Bonferroni-Holm correction. Although circumferential calf compression serves as a reasonable analog for muscle pressurization due to isometric muscle contraction, it may not mimic in vivo muscle shape changes. The stent design investigated in this study was a cobalt-chromium coronary stent, and its deformations may not be indicative of other designs. Although self-expanding nitinol stents are more often used in the peripheral vasculature, such as in the carotid, iliac, femoral, and popliteal arteries, tibial arteries are most often stented with cobalt-chromium coronary stents due to commercial availability and stent sizes. Finally, note that numerous joint and compression manipulations were performed serially in the same order on each leg specimen and that deformations attributed to a particular motion may have contributions from prior manipulations, potentially causing accumulation of deformation for latter manipulations.

Conclusion

A cadaver model was developed to quantify tibial artery stent deformations due to ankle plantarflexion, ankle dorsiflexion, knee flexion, and simulated calf muscle contraction. Due to ankle and knee joint motion, there is stent diametric crush in the posterior tibial and peroneal arteries, likely due to their location in the deep posterior compartment, which is adjacent to the large soleus and gastrocnemius muscles in the calf that can bulge with joint motion. Stent diametric crush in the posterior tibial artery is more dramatic for knee flexion and calf compression compared to ankle motion, potentially because the higher bone-to-muscle ratio near the ankle protects against diametric crush. Due to knee flexion and calf compression, ostium-crossing stents experience an order of magnitude higher axial length change compared to those exclusively in the anterior tibial, posterior tibial, or peroneal arteries, probably because stents with more oblique orientation are more impacted by forces perpendicular to the long axis of the leg. No significant stent bending was observed due to any leg motion, likely because the stents were implanted in the midcalf, situated away from both the knee and ankle joints and protected from bending by the rigid tibia and fibula. The stent deformations quantified in this study can guide tibial vessel device development and anatomic site selection for interventionalists and indications for use.

Declaration of competing interest

Christopher P. Cheng and Stanley K. Zimmerman were previously paid consultants to Medtronic but have not been so for over 4 years. Johan Bondesson and Anna Johnson have no conflicts to disclose.

Funding sources

The cadaver study was partially funded by Medtronic, which also provided devices; however, Medtronic had no involvement in the study design or collection, analysis, and interpretation of data, or decision to submit the manuscript for publication.

Ethics statement and patient consent

This article does not report on patients or patient data. Ethical approval and patient consent were not required.

References

1. Fowkes FG, Rudan D, Rudan I, et al. Comparison of global estimates of prevalence and risk factors for peripheral artery disease in 2000 and 2010: a systematic review and analysis. *Lancet*. 2013;382(9901):1329–1340. https://doi.org/10.1016/S0140-6736(13)61249-0
2. Society for Vascular Surgery Lower Extremity Guidelines Writing Group, Conte MS, Pomposelli FB, et al. Society for Vascular Surgery practice guidelines for atherosclerotic occlusive disease of the lower extremities: management of asymptomatic disease and claudication. *J Vasc Surg*. 2015;61(3 Suppl):2S–41S. Published correction appears in *J Vasc Surg*. 2015;61(5):1382.
3. Zilinyi RS, Alsaloum M, Snyder DJ, et al. Surgical and endovascular therapies for below-the-knee peripheral arterial disease: a contemporary review. *J Soc Cardiovasc Angiogr Interv*. 2024;3(3):101268. https://doi.org/10.1016/j.jscai.2023.101268
4. Conte MS, Bradbury AW, Kolh P, et al. Global vascular guidelines on the management of chronic limb-threatening ischemia. *J Vasc Surg*. 2019;69(6S):3S–125S.e40. Published correction appears in *J Vasc Surg*. 2019;70(2):662.
5. Li J, Varcoe R, Manzi M, et al. Below-the-knee endovascular revascularization: a position statement. *JACC Cardiovasc Interv*. 2024;17(5):589–607. https://doi.org/10.1016/j.jcin.2023.11.040
6. Changal K, Patel M, Devarasetty PP, et al. Drug-eluting stents versus conventional endovascular therapies in symptomatic infrapopliteal peripheral artery disease: a meta-analysis. *J Soc Cardiovasc Angiogr Interv*. 2022;1(2):100024. https://doi.org/10.1016/j.jscai.2022.100024
7. Biscaglia S, Tebaldi M, Tumscitz C, et al. Prospective identification of stent fracture by enhanced stent visualization system during percutaneous coronary intervention. *Circ J*. 2016;81(1):82–89. https://doi.org/10.1253/circj.CJ-16-0785

8. Scheinert D, Scheinert S, Sax J, et al. Prevalence and clinical impact of stent fractures after femoropopliteal stenting. *J Am Coll Cardiol*. 2005;45(2):312–315. https://doi.org/10.1016/j.jacc.2004.11.026
9. Higashiura W, Kubota Y, Sakaguchi S, et al. Prevalence, factors, and clinical impact of self-expanding stent fractures following iliac artery stenting. *J Vasc Surg*. 2009; 49(3):645–652. https://doi.org/10.1016/j.jvs.2008.10.019
10. Zhang W, Gao X, Zhang H, et al. Maglev-fabricated long and biodegradable stent for interventional treatment of peripheral vessels. *Nat Commun*. 2024;15(1):7903. https://doi.org/10.1038/s41467-024-52288-4
11. Suh GY, Beygui RE, Fleischmann D, Cheng CP. Aortic arch vessel geometries and deformations in patients with thoracic aortic aneurysms and dissections. *J Vasc Interv Radiol*. 2014;25(12):1903–1911. https://doi.org/10.1016/j.jvir.2014.06.012
12. Robertson SW, Cheng CP, Razavi MK. Biomechanical response of stented carotid arteries to swallowing and neck motion. *J Endovasc Ther*. 2008;15(6):663–671. https://doi.org/10.1583/08-2528.1
13. Suh GY, Choi G, Herfkens RJ, Dalman RL, Cheng CP. Three-dimensional modeling analysis of visceral arteries and kidneys during respiration. *Ann Vasc Surg*. 2016;34: 250–260. https://doi.org/10.1016/j.avsg.2016.04.004
14. Cheng CP, Choi G, Herfkens RJ, Taylor CA. The effect of aging on deformations of the superficial femoral artery resulting from hip and knee flexion: potential clinical implications. *J Vasc Interv Radiol*. 2010;21(2):195–202. https://doi.org/10.1016/j.jvir.2009.08.027
15. Gökgöl C, Schumann S, Diehm N, Zheng G, Büchler P. In vivo quantification of the deformations of the femoropopliteal segment: percutaneous transluminal angioplasty vs nitinol stent placement. *J Endovasc Ther*. 2017;24(1):27–34. https://doi.org/10.1177/1526602816677530
16. MacTaggart J, Poulson W, Seas A, et al. Stent design affects femoropopliteal artery deformation. *Ann Surg*. 2019;270(1):180–187. https://doi.org/10.1097/SLA.0000000000002747
17. Cheng CP, Dua A, Suh GY, Shah RP, Black SA. The biomechanical impact of hip movement on iliofemoral venous anatomy and stenting for deep venous thrombosis. *J Vasc Surg Venous Lymphat Disord*. 2020;8(6):953–960. https://doi.org/10.1016/j.jvsv.2020.01.022
18. Macias BR, D'Lima DD, Cutuk A, et al. Leg intramuscular pressures and in vivo knee forces during lower body positive and negative pressure treadmill exercise. *J Appl Physiol (1985)*. 2012;113(1):31–38. https://doi.org/10.1152/japplphysiol.01434.2011
19. Cheng CP. *Handbook of Vascular Motion*. 1st ed. Elsevier; 2019.
20. Katsanos K, Diamantopoulos A, Spiliopoulos S, Karnabatidis D, Siablis D. Below-the-ankle angioplasty and stenting for limb salvage: anatomical considerations and long-term outcomes. *Cardiovasc Intervent Radiol*. 2013;36(4):926–935. https://doi.org/10.1007/s00270-012-0514-x
21. Karnabatidis D, Katsanos K, Spiliopoulos S, Diamantopoulos A, Kagadis GC, Siablis D. Incidence, anatomical location, and clinical significance of compressions and fractures in infrapopliteal balloon-expandable metal stents. *J Endovasc Ther*. 2009;16(1):15–22. https://doi.org/10.1583/08-2530.1
22. Alimi YS, Barthelemy P, Juhan C. Venous pump of the calf: a study of venous and muscular pressures. *J Vasc Surg*. 1994;20(5):728–735. https://doi.org/10.1016/s0741-5214(94)70160-1
23. Ballard RE, Watenpaugh DE, Breit GA, Murthy G, Holley DC, Hargens AR. Leg intramuscular pressures during locomotion in humans. *J Appl Physiol (1985)*. 1998;84(6):1976–1981. https://doi.org/10.1152/jappl.1998.84.6.1976
24. Wilson N, Wang K, Dutton RW, Taylor C. A software framework for creating patient specific geometric models from medical imaging data for simulation based medical planning of vascular surgery. In: Niessen WJ, Viergever MA, eds. *Medical Image Computing and Computer-Assisted Intervention – MICCAI 2001. MICCAI 2001. Lecture Notes in Computer Science*. 2208. Springer; 2001:449–456.
25. Choi G, Cheng CP, Wilson NM, Taylor CA. Methods for quantifying three-dimensional deformation of arteries due to pulsatile and nonpulsatile forces: implications for the design of stents and stent grafts. *Ann Biomed Eng*. 2009; 37(1):14–33. https://doi.org/10.1007/s10439-008-9590-0
26. Choi G, Xiong G, Cheng CP, Taylor CA. Methods for characterizing human coronary artery deformation from cardiac-gated computed tomography data. *IEEE Trans Bio Med Eng*. 2014;61(10):2582–2592. https://doi.org/10.1109/TBME.2014.2323333
27. Cheng CP, Bondesson J, Bendavid J, Haulon S. Renovisceral artery alterations due to branched endovascular aortic repair and respiratory-induced deformations. *J Vasc Surg*. 2023;78(4):902–911. https://doi.org/10.1016/j.jvs.2023.05.032
28. Holm A. A simple sequentially rejective multiple test procedure. *Scand J Stat*. 1979; 6:65–70.
29. Wallensten R, Eriksson E. Intramuscular pressures in exercise-induced lower leg pain. *Int J Sports Med*. 1984;5(1):31–35. https://doi.org/10.1055/s-2008-1025877
30. Avisse C, Marcus C, Ouedraogo T, Delattre JF, Menanteau B, Flament JB. Anatomo-radiological study of the popliteal artery during knee flexion. *Surg Radiol Anat*. 1995;17(3):255–262. https://doi.org/10.1007/BF01795060
31. Vu HTT, Gomez F, Cherelle P, Lefeber D, Nowé A, Vanderborght B. ED-FNN: a new deep learning algorithm to detect percentage of the gait cycle for powered prostheses. *Sensors (Basel)*. 2018;18(7):2389. https://doi.org/10.3390/s18072389